FEM-based Dynamic Model for Cable-Driven Parallel Robots with Elasticity and Sagging

Karim Moussa, Eulalie Coevoet, Christian Duriez, Maxime Thieffry, Fabien Claveau, Philippe Chevrel, Stéphane Caro

▶ **To cite this version:**

Karim Moussa, Eulalie Coevoet, Christian Duriez, Maxime Thieffry, Fabien Claveau, et al.. FEM-based Dynamic Model for Cable-Driven Parallel Robots with Elasticity and Sagging. CableCon 2023: 6th International Conference on Cable-Driven Parallel Robots, Jun 2023, Nantes, France. 10.1007/978-3-031-32322-5_5 . hal-04037333

HAL Id: hal-04037333
https://hal.science/hal-04037333v1

Submitted on 20 Mar 2023

HAL is a multi-disciplinary open access archive for the deposit and dissemination of scientific research documents, whether they are published or not. The documents may come from teaching and research institutions in France or abroad, or from public or private research centers.

L'archive ouverte pluridisciplinaire **HAL**, est destinée au dépôt et à la diffusion de documents scientifiques de niveau recherche, publiés ou non, émanant des établissements d'enseignement et de recherche français ou étrangers, des laboratoires publics ou privés.

FEM-based Dynamic Model for Cable-Driven Parallel Robots with Elasticity and Sagging*

Karim Moussa[1,3], Eulalie Coevoet[2], Christian Duriez[2], Maxime Thieffry[3], Fabien Claveau[3], Philippe Chevrel[3], and Stéphane Caro[3]

[1] Nantes Université, IRT Jules Verne, LS2N, UMR 6004, F-44000, Nantes , France
karim.moussa@irt-jules-verne.fr
[2] Université de Lille, INRIA, CNRS, CRIStAL UMR CNRS 9189, Lille, France
[3] IMT Atlantique, Nantes Université, École Centrale de Nantes, CNRS, LS2N, UMR 6004, F-44000 Nantes, France.

Abstract. Cable-Driven Parallel Robots (CDPRs) are a type of robot that is growing in popularity for different kinds of applications. However, the use of cables instead of rigid links makes the modelling of this robot a complex task, and therefore their trajectory planning and control are challenging. Assumptions such as inelastic, massless and non-sagging cables made when the CDPR is small are no longer valid when the robot becomes large. This paper presents a CDPR dynamic model taking into account cable elasticity and sagging, and its implementation within an open-source framework, named SOFA. Finally, the simulation results are compared to experiments conducted on a suspended CDPR.

Keywords: Cable-Driven Parallel Robots · Dynamic Modeling · Finite Element Method · Cable Model · Beam Theory

1 Introduction

Cable-Driven Parallel Robots (CDPRs, see Fig. 1) are used to perform operations in a very large workspace: from the assembly of solar panels [1] to flight simulators [2], through the development of a large radio telescope [3]. Simulating this kind of robots is of interest for carrying out potentially dangerous or time-consuming tests, such as the analysis and prediction of their behaviour, e.g. during their design and the synthesis of control laws, or to conduct tests at the safety limits, i.e. failure tests of actuator and cable breakage. It can also make it possible to estimate certain parameters or variables that cannot be measured on a real system. To do so, dynamic models that are both precise and computationally tractable are mandatory.

Several cable models are available in the literature as shown in Fig. 2. A first level of dynamic modeling is assuming massless, straight or non elastic cables [5, 6]. Some works consider elastic, but massless cables, therefore not undergoing

* This work is supported by both IRT Jules Verne in the framework of the PERFORM program and the EquipEx+ TIRREX project, grant ANR-21-ESRE-0015.

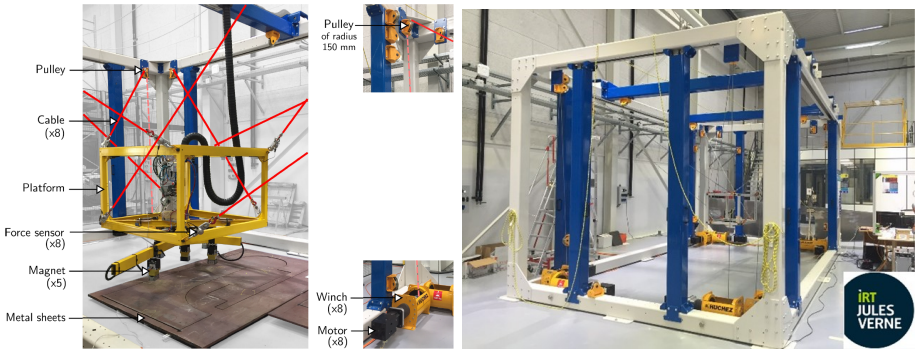

Fig. 1: CDPR (CAROCA) located at IRT Jules Verne, from [4].

cable sagging [7]. This may be of interest to model synthetic cables that have low mass density. In [8], the authors used the assumed mode approach to model a three degree-of-freedom (DOF) CDPR with sagging and non-elastic cables. The Irvine model [9] offers the possibility to model faithfully the cable geometry taking into account cable sag and elasticity, but only in the static case. Besides, it neglects the bending stiffness of the cable. It is therefore not directly suitable for dynamic control applications. Recently, a Rayleigh-Ritz cable model that takes into account the variation in cable mass and stiffness was studied in [10]. However, results are for now limited to a single DOF CDPR.

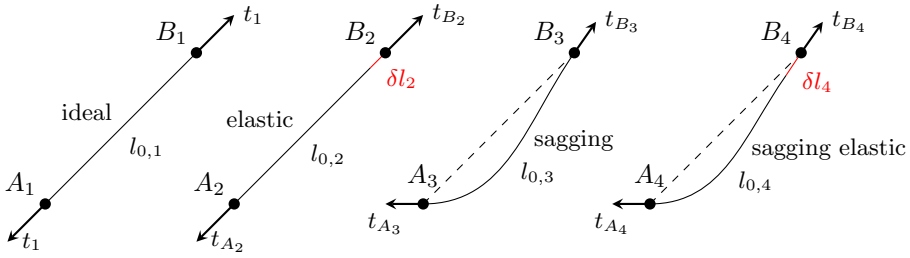

Fig. 2: Illustration of different cable models.

It should be noted that few CDPR simulators exist in the literature based on different cable models. In [11], a massless and inextensible cable model is implemented in Gazebo and ROS to simulate CDPR dynamic behaviour. Multiple nodes of Reissner beam are used in [12] to model cable elasticity, sag, shear and torsion in the XDE framework. However, some of the physical parameters of the cable such as the Young modulus need to be adapted in order to ensure simulation stability. The simulation time obtained in [12] is slow for testing and tuning controllers, namely, 10 h to simulate 10 s. CoppeliaSim offers elastic, but

straight and massless cables [13]. Other frameworks like AGX Dynamics [14] and MapleSim [15] make it possible to consider elasticity and cable mass with a lumped parameter discretization.

This work proposes a cable model suitable for CDPR control design. The proposed dynamic model considers both cable elasticity and sag. This dynamic model is implemented in SOFA framework [16], which was developed for finite element modeling and simulation of soft objects. A digital twin of CAROCA, a CDPR located at IRT Jules Verne, is developed in SOFA. The results from the simulation with SOFA are compared to the results from simulators developed with Maplesoft™ MapleSim software.

The paper is organized as follows: Section 2 describes the cable model obtained based on the FEM model of beams in SOFA and its application to a suspended CDPR. Results from SOFA and MapleSim simulations are compared with experimental results in Section 3. Conclusions and future work are drawn in Section 4.

2 CDPR Dynamic Modeling

This section presents the dynamic model of CDPRs including both cable elasticity and sagging. The presented methodology is intended to be as generic as possible and is valid for all configurations (suspended and fully-constrained), but will be illustrated throughout the paper with a suspended CDPR. The method relies on the finite element method (FEM) implemented within the SOFA framework, a physics-based simulation platform that uses FEM to model, simulate, and control deformable objects.

2.1 FEM Model of Beams in SOFA

This method, first presented for SOFA in [17], relies on a representation based on three-dimensionnal Timoschenko beam theory [18] and a specific corotational formulation to account for large displacements [19, 20]. It is implemented within the BeamAdapter[4] plugin of the SOFA framework.

The beam is discretized into $\mathcal{N}$ small elements, each of them corresponding to the one depicted in Fig. 3(a). The motion of the flexible beam is then decomposed into two parts, a rigid body motion and a deformation motion, with the assumption that the deformation remains small at the level of each elements. The equation of motion of an object according to Newton's second law is given by:

$$\mathbf{M}\ddot{\mathbf{q}} = \mathbf{f}_{\mathrm{e}}(\mathbf{q}, \dot{\mathbf{q}}) + \mathbf{H}(\mathbf{q})\lambda \tag{1}$$

where $\mathbf{q} \in \mathbb{R}^n$ is the vector of generalized coordinates, $\mathbf{M} \in \mathbb{R}^{n\times n}$ is the inertia matrix of the system and $\mathbf{f}_{\mathrm{e}}(\mathbf{q}, \dot{\mathbf{q}}) : \mathbb{R}^n \times \mathbb{R}^n \to \mathbb{R}^n$ gathers external forces. Finally, $\mathbf{H}(\mathbf{q}) : \mathbb{R}^n \to \mathbb{R}^{n\times m}$ is the Jacobian matrix that gives the direction of constraints forces, $\lambda \in \mathbb{R}^m$ the vector of Lagrange multipliers corresponding to

[4] https://github.com/sofa-framework/BeamAdapter

the constraints and m is the number of algebric constraints. In the case of a beam element, $\mathbf{q} = (\mathbf{q}_a^T, \mathbf{q}_b^T)^T$ where indices a and b represent the extremities of the beam element as shown in Fig. 3(a), $\mathbf{q}_a$ and $\mathbf{q}_b$ contain a positional vector $\in \mathbb{R}^3$ and a rotational term $\in$ SO(3) defining the pose of each extremity. $\mathbf{M}$ is given in [18] and depends on the second moments of area I_y and I_z with respect to the axes y and z respectively, the cable cross section area A, the length of the beam element L, the second polar moment of area J, and the material density ρ.

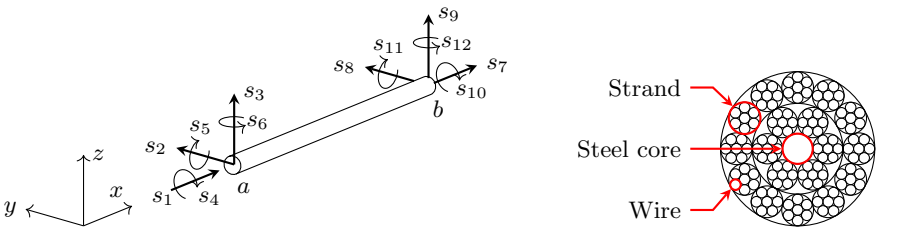

(a) A single beam element.

(b) Cable structure used for the CAROCA robot.

Fig. 3: Cable discretization.

With the corotational assumption, the deformation in the cable elements is small locally and the external force can be calculated with the linear relation:

$$\mathbf{f}_e(\mathbf{q}) = \mathbf{K}(\mathbf{u}(\mathbf{q}) - \overline{\mathbf{u}(\mathbf{q})}) \tag{2}$$

where $\mathbf{u}(\mathbf{q})$ is the deformed configuration of $\mathbf{q}$, $\overline{\mathbf{u}(\mathbf{q})}$ is the rest configuration of $\mathbf{q}$, both expressed in the local frame, and $\mathbf{K}$ is the stiffness matrix given in Eq. (3).

$$\mathbf{K} = \begin{bmatrix}
\frac{EA}{L} & & & & & & & & & & & \\
0 & \frac{12EI_z}{L^3\phi_y} & & & & & & & & & & \\
0 & 0 & \frac{12EI_y}{L^3\phi_z} & & & & & & & & & \\
0 & 0 & 0 & \frac{GJ}{L} & & & & & & & & \\
0 & 0 & -\frac{6EI_y}{L^2\phi_z} & 0 & \frac{EI_y\Phi_{pz}}{L\phi_z} & & & & & & & \\
0 & \frac{6EI_z}{L^2\phi_y} & 0 & 0 & 0 & \frac{EI_z\Phi_{py}}{L\phi_y} & & & & & & \\
-\frac{EA}{L} & 0 & 0 & 0 & 0 & 0 & \frac{EA}{L} & & & & & \\
0 & -\frac{12EI_z}{L^3\phi_y} & 0 & 0 & 0 & -\frac{6EI_z}{L^2\phi_y} & 0 & \frac{12EI_z}{L^3\phi_y} & & & & \\
0 & 0 & -\frac{12EI_y}{L^3\phi_z} & 0 & \frac{6EI_y}{L^2\phi_z} & 0 & 0 & 0 & \frac{12EI_y}{L^3\phi_z} & & & \\
0 & 0 & 0 & -\frac{GJ}{L} & 0 & 0 & 0 & 0 & 0 & \frac{GJ}{L} & & \\
0 & 0 & -\frac{6EI_y}{L^2\phi_z} & 0 & \frac{EI_y\Phi_{nz}}{L\phi_z} & 0 & 0 & 0 & \frac{6EI_y}{L^2\phi_z} & 0 & \frac{EI_y\Phi_{pz}}{L\phi_z} & \\
0 & \frac{6EI_z}{L^2\phi_y} & 0 & 0 & 0 & \frac{EI_z\Phi_{ny}}{L\phi_y} & 0 & -\frac{6EI_z}{L^2\phi_y} & 0 & 0 & 0 & \frac{EI_z\Phi_{py}}{L\phi_y}
\end{bmatrix} \tag{3}$$

where $\Phi_{py} = 3+\phi_y$, $\Phi_{ny} = 3-\phi_y$, $\phi_y = 1+\dfrac{12EI_z}{GA_{sy}L^2}$, $\Phi_{pz} = 3+\phi_z$, $\Phi_{nz} = 3-\phi_z$, $\phi_z = 1+\dfrac{12EI_y}{GA_{sz}L^2}$, $G = \dfrac{E}{2(1+\mu)}$, E is the Young's modulus, μ is the Poisson's ration, and A_{sy} and A_{sz} are the actual surfaces of the cable due to shear along the y and z directions.
In CDPR use cases, the sheering can be neglected and therefore $\phi_y = \phi_z = 1$. The cables have a symmetrical cross-section and therefore $I_y = I_z = I$. Once the external force $\mathbf{f}_e(\mathbf{q})$ is calculated in the local frame, it is transformed to the global frame using the rotation matrix of the local frame.

The model presented in [18] is used to model beams. However, compared to beams, a cable can bend more and is unable to withstand compression force. This difference is mainly due to the second moment of area I that is smaller for a cable. The structure of the cable used for the CAROCA robot is shown in Fig. 3(b), it is a two layers concentric contra-helical cable made of steel where cable strands have opposite lay directions. As shown in [21], when the cable is straight all the wires are sticking together and act as a one homogeneous body that can bend around the central axis of the cable. The quadratic moment is at its maximum I_{max}. However, when the curvature k of the cable increases the wires start to slip and eventually at the most extreme case each wire bends around its own axis. The quadratic moment is then at its minimum I_{min} defined as:

$$I_{min} = I_c + \sum_{i=1}^{n_s} I_{s_{min},i} \cos\beta_{s,i} \tag{4}$$

where I_c is the quadratic moment of the steel core around its own axis, $I_{s_{min},i}$ is the minimum quadratic moment of strand i around its own axis calculated with Eq. (4) after replacing strand with wire, $\beta_{s,i}$ is the lay angle of strand i and n_s is the number of strands. Then, I_{max} can be calculated:

$$I_{max} = I_{min} + \sum_{i=1}^{a} \frac{n_i}{2} A_i r_i^2 \cos^3\beta_{l,i} \tag{5}$$

where n_i is the number of strands in layer i, A_i is the cross section area of each strand in layer i, r_i is the radius of layer i, $\beta_{l,i}$ is the lay angle of the strands in layer i and a is the number of layers. Note that I_{min} and I_{max} are independent from the curvature of the cable and its tension force value.
To simplify the model, a constant value for $I \in [I_{min}, I_{max}]$ will be chosen. Knowing the working region of the cable (e.g. assuming that the curvature will not reach significant values as much as $k = 1\text{m}^{-1}$), and based on the identified transition function between EI_{max} and EI_{min} in [21] shown in Fig. 4, the parameter $\alpha = 0.65$ is chosen such that:

$$I = I_{min} + \alpha(I_{max} - I_{min}) \tag{6}$$

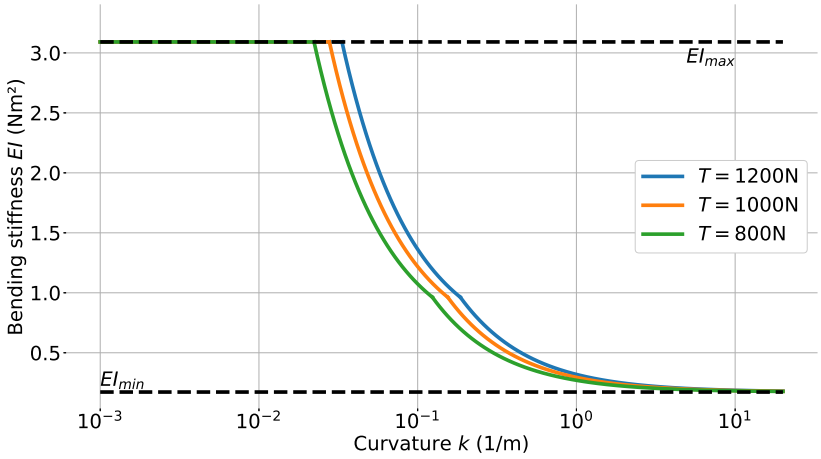

Fig. 4: Theoretical evolution of bending stiffness EI as function of the curvature k for different tension T values, based on [21].

2.2 Application to CDPRs

In CDPRs, the cables are attached at one end to the platform using spherical joint-equivalent connectors and are rolled at the other end around the winches. The cables can be oriented by passing through pulleys to change the CDPR configuration from suspended to fully-constrained. In addition to cables, pulleys and winches have an influence on the full model of the CDPR. Their impact varies depending on their dimensions and the friction they induce. To get the full CDPR model, each cable is modeled by Eq. (1) where the constraints represent the connection between the cable and the platform, and its contact with the pulley and the winch. The spherical joint does not transmit torque, therefore only position constraints are applied. A 6-DOF, 2-DOF, and 1-DOF dynamic models for the platform, the pulley, and the winch, respectively are implemented. The cable/pulley, cable/winch and gearhead frictions are neglected. In the following section, the different simulations are compared with the experimental results.

3 Comparison with Existing Simulators

3.1 Modeled robot

For this first trial, the implemented model in SOFA described in Sec. 2.1 is compared to other state-of-the-art models ("Rope" and "Cable" described in Sec. 3.2) of the simulation software MapleSim, and to real-robot measurements from the CAROCA experimental platform (see Fig. 1). It is a suspended CDPR with 8 cables allowing 6-DOF for the platform. Steel cables (see Fig. 3(b)) are used, they can withstand significant tensions (10 kN), but can present significant sags given their mass. The working area of the robot is 7 m $\times$ 4 m $\times$ 3 m. The moving platform's dimensions are 1.5 m $\times$ 1.5 m $\times$ 1 m, and it weighs 366 kg.

3.2 MapleSim

The MapleSim [15] software provides some tools to model cable-driven robots including cable models, pulleys, and winches. This framework provides three possible models : rope, chain and cable. Rope is the simplest one where only the elasticity is considered, and cable is the most accurate where elasticity and sagging are considered. The rope model is made up of two massless nodes connected by a spring and a damper. The cable model relies on [22], where the cable is discretized into $\mathcal{N}$ equidistant nodes, being connected with each other by springs and dampers. Moreover, the cable mass is spread along the nodes. These first trials proposed in this paper are dedicated to these two models, they will serve as a reference to compare with SOFA's implemented cable model's results.

3.3 Definition of scenario

The pick-and-place trajectory used to compare the simulators with respect to the experimental results is depicted in Figs. 5 and 6. Using an ideal cable model (massless and rigid), an inverse geometric model (IGM) and an inverse kinematic model (IKM) allow to find the desired joint space, i.e. the winches, angular position $\boldsymbol{\theta}_d$ and velocity $\dot{\boldsymbol{\theta}}_d$, as shown in Fig. 7. Then, a PD controller is used to calculate the winch torques $\boldsymbol{\tau}_w$ and track the reference trajectory. Controller gains in simulators are tuned slightly different than the robot as they must compensate for the friction [6].

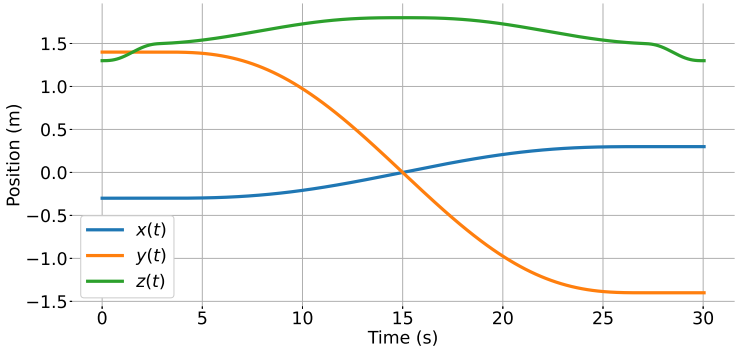

Fig. 5: Reference Cartesian trajectory of the robot platform.

3.4 Simulation Results

The parameters needed to simulate the models (BeamAdapter in SOFA, rope and cable in MapleSim) and their values are shown in Table 1. C_a is the cable's axial damping and d_r is its bending damping ratio. As said before, the sheer is

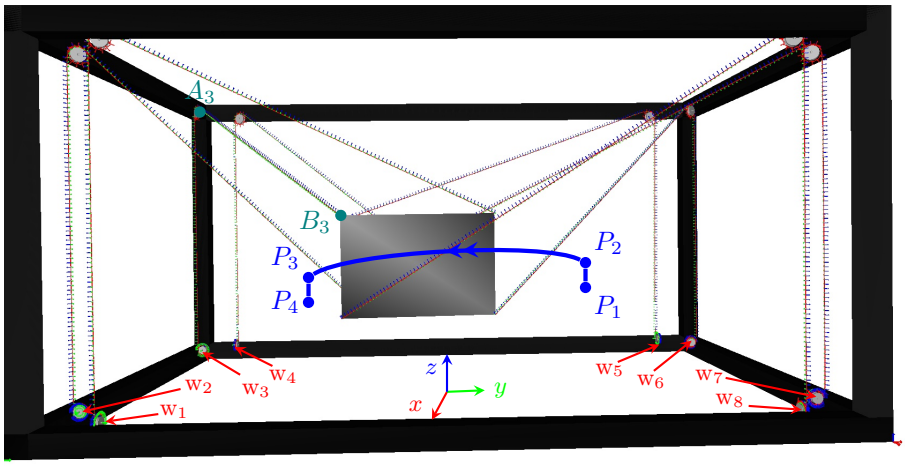

Fig. 6: Viewing environment in SOFA with added winch numbering w_i and the reference Cartesian trajectory of the platform from P_1 to P_4.

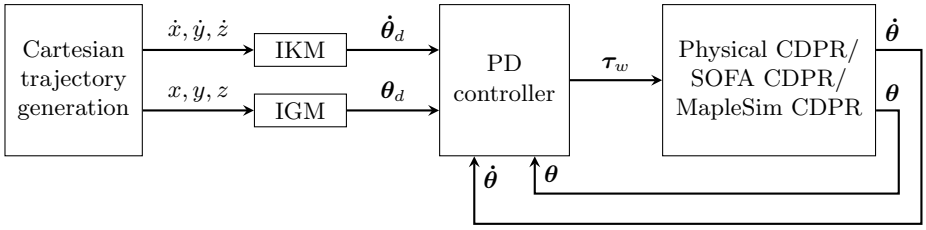

Fig. 7: Trajectory generation and control architecture.

Table 1: Tuning parameters associated to each cable model.

Parameters / Models	E ($\times 10^{11}$Pa)	μ	A ($\times 10^{-5}$m^2)	ρ (kg m^{-3})	C_a ($\times 10^{9}$N s m^{-1})	d_r	α
BeamAdapter	1.022	0.28	2.1488	7850	-	-	0.65
Rope	1.022	-	2.1488	-	22.8	-	-
Cable	1.022	-	2.1488	7850	22.8	0.12	-

negligible in CDPR applications and so the precision of Poisson's ratio's value has no impact on the simulation.

The first ten seconds of simulations have been cut on the results depicted in Figs. 8 to 11 ; they are associated to the initialisation of the robot, where the platform is kept at the initial target Cartesian position. This transitory behaviour before reaching the static equilibrium is not of interest. Then, the 30s trajectory shown in Fig. 5 is applied.

The measured cable tensions at the platform from both frameworks are compared to the experimental measures of the force sensors located between the cables and the moving-platform (MP). The resulting plots for cables 6 and 7 are shown in Fig. 8. The remaining six cables behave in a similar manner.

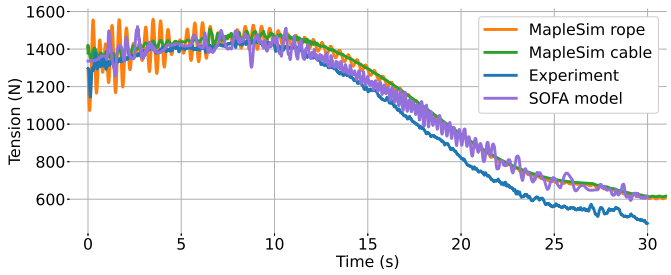

(a) Cable 6

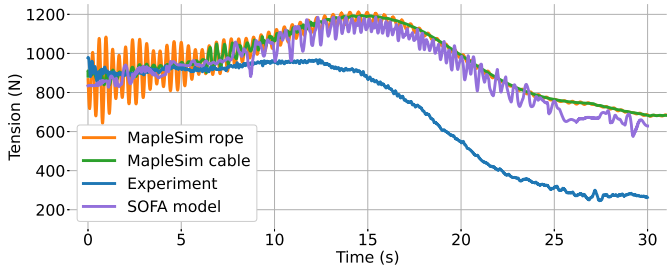

(b) Cable 7

Fig. 8: Comparison between simulated and measured cable tensions.

It appears that the plots of both models in MapleSim are almost identical. This is probably due to the weight of the cable being insufficient to make a difference under the current cable tension between the massless (rope) and non-massless (cable) models, and therefore the cables are almost straight. A small oscillation for the rope model is noticed, the PD controller gains might be high for this model. The plots of SOFA's model match those of MapleSim. However, these three models have the following divergence with the experimental results. On one side, tensions in cables 2, 4, 6, and 8 match the experiment measurements. On the other side, they converge to a value different from the measured one in cables 1, 3, 5, and 7. This causes high Relative Root Mean Squared Errors (RRMSE) of some simulated cables tensions with respect to the the experiment ($> 20\%$) as can be seen in Fig. 9. The order of the cables and winches is given in Fig. 6. The SOFA model has slightly lower RRMSE mean value compared to MapleSim. As a first explanation, because of the redundancy of actuation, multiple set of cables tensions can result in the same platform position. A common distribution

algorithm should be implemented in the three simulators and the experimental setup to handle this aspect.

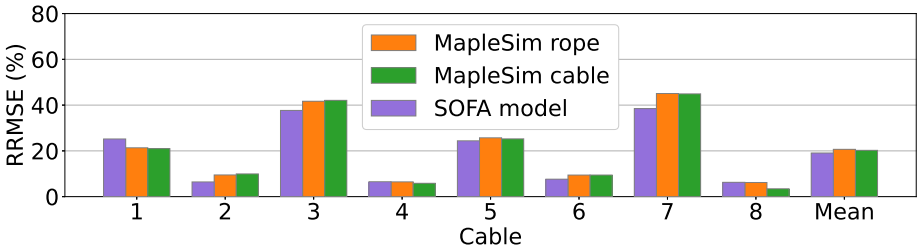

Fig. 9: RRMSE (%) for each cable tension.

As for the winches, the angular position of winch 6 is shown in Fig. 10. The plots of the remaining 7 being similar.

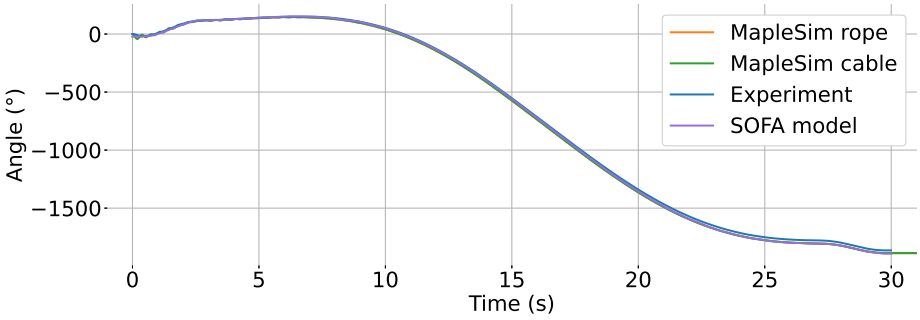

Fig. 10: Angular position of winch 6.

Contrary to the cables tensions, the plots of the three simulated models match the experimental measurements. This is due to the controller being implemented in the joint space and not considering the cable tension. This can be seen in Fig. 11 where all RRMSE are very small ($< 5\%$) with respect to the the experiment, with a slight advantage in mean value for MapleSim models.

The simulation time for every model varies and is given in Table 2. The solver used in MapleSim is a variable step solver (Rosenbrock). In SOFA, a fixed step solver was used (implicit Euler) with a time step of dt equal to $0.005s$.

Ultimately, the SOFA model presents a computational burden far less important than the Maplesim cable model, while it permits to simulate more internal degrees of freedom; 294 nodes in SOFA versus 7 in MapleSim.

As the mass of the cable increases (longer cables or heavier material), the applied motor torque must be increased to keep the cables as straight as possible.

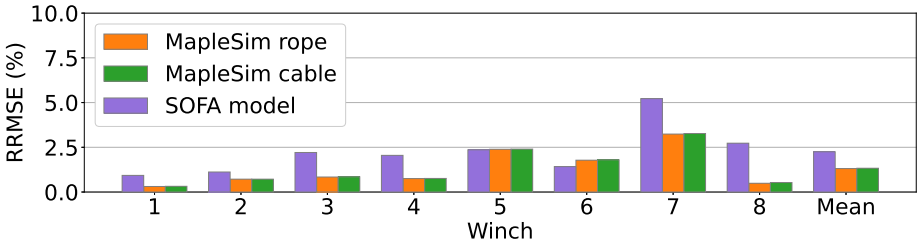

Fig. 11: RRMSE (%) for each winch angular position.

Table 2: Simulation time for different models.

	MapleSim rope	MapleSim cable	Sofa model
Time	20 min	12 h	45 min

Nevertheless, this might not be possible because of security or power consumption limit. To verify the capacity of the proposed simulator to model the sagging, another simulation was run where the winch 1 was locked at its initial position. The MP pose and the shape of the cables at the end of the simulation are illustrated in Fig. 12.

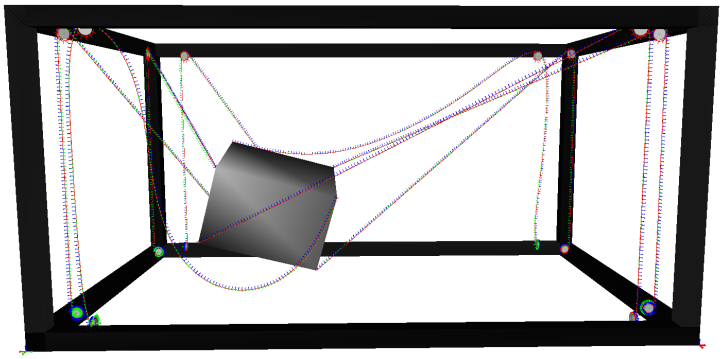

Fig. 12: The pose of the platform and the state of the cables (sagging) at $t = 30s$ when winch 1 is locked.

The rolled cable on winch 1 has an important sagging. The rolled cable on winch 5 shows also non negligible sagging due to the orientation of the platform that makes the attach point closer than the planed one. These very first results demonstrate that the SOFA model makes it possible to simulate important cable sagging. Further tests will be conducted on the robot to evaluate the precision of the simulation's sag.

The attached video in SOFA shows the vibrations of the cables but not much sagging in the first simulation. The sagging appears clearly in the second simulation. It can be found online at: https://youtu.be/uUwP0CZeMqo.

4 Conclusion and Perspectives

This paper dealt with the modeling and simulation of cable-driven parallel robots (CDPRs). Specifically, the model sought must account for the effects of cable sag and elasticity. Although ambitious in terms of the realism targeted, the complexity of the model must remain limited. The approach followed is that of the use of three-dimensional beam theory [18] and corotational method [19]. The model was implemented using finite element method within a physics-based simulation platform, the SOFA framework. To evaluate the proposed model, the simulation results were compared with real data obtained on the CAROCA CDPR experimental platform, but also with other simulation results obtained from a model implemented using MapleSim software and the MapleSim Ropes and Pulleys Library. The cable tensions, as well as the angular positions of the winches were compared. The proposed model was implemented in SOFA and proved to be as accurate as the model implemented in MapleSim. It should be noted that it is faster than the MapleSim cable model, but slower than the MapleSim massless rope model. Therefore, it is more advantageous in applications where sag is greater.

The perspectives relate to the use of other cable models [23, 24], still within the SOFA framework, to model CDPRs. In particular, the theory of Cosserat [24] will be considered to model the cables. Finally, the code of the simulator will be available in open source.

References

1. Pott, A., Meyer, C., Verl, A.: Large-scale assembly of solar power plants with parallel cable robots. In: ISR 2010 (41st International Symposium on Robotics) and ROBOTIK 2010 (6th German Conference on Robotics). pp. 1–6. VDE (2010)
2. Miermeister, P., Lächele, M., Boss, R., Masone, C., Schenk, C., Tesch, J., Kerger, M., Teufel, H., Pott, A., Bülthoff, H.H.: The cablerobot simulator large scale motion platform based on cable robot technology. In: 2016 IEEE/RSJ International Conference on Intelligent Robots and Systems (IROS). pp. 3024–3029. IEEE (2016)
3. Tang, X., Yao, R.: Dimensional design on the six-cable driven parallel manipulator of fast. Journal of Mechanical Design **133**(11) (2011)
4. Picard, E., Caro, S., Claveau, F., Plestan, F.: Pulleys and force sensors influence on payload estimation of cable-driven parallel robots. In: 2018 IEEE/RSJ International Conference on Intelligent Robots and Systems (IROS). pp. 1429–1436 (Oct 2018). https://doi.org/10.1109/IROS.2018.8594171
5. Santos, J.C., Chemori, A., Gouttefarde, M.: Model predictive control of large-dimension cable-driven parallel robots. In: International Conference on Cable-Driven Parallel Robots. pp. 221–232. Springer (2019)

6. Picard, E., Tahoumi, E., Plestan, F., Caro, S., Claveau, F.: A new control scheme of cable-driven parallel robot balancing between sliding mode and linear feedback. IFAC-PapersOnLine **53**(2), 9936–9943 (2020). https://doi.org/10.1016/j.ifacol.2020.12.2708, 21st IFAC World Congress
7. Baklouti, S., Courteille, E., Caro, S., Dkhil, M.: Dynamic and oscillatory motions of cable-driven parallel robots based on a nonlinear cable tension model. Journal of mechanisms and robotics **9**(6), 061014 (2017)
8. Saadaoui, R., Laroche, E., Bara, I., Piccin, O.: H∞ control of a planar 3-dof flexible-cable manipulator. IFAC-PapersOnLine **55**, 199–204 (10 2022). https://doi.org/10.1016/j.ifacol.2022.09.347
9. Merlet, J.P.: Some properties of the irvine cable model and their use for the kinematic analysis of cable-driven parallel robots. Mechanism and Machine Theory **135**, 271–280 (2019)
10. Godbole, H.A., Caverly, R.J., Forbes, J.R.: Dynamic modeling and adaptive control of a single degree-of-freedom flexible cable-driven parallel robot. Journal of Dynamic Systems, Measurement, and Control **141**(10) (2019)
11. Okoli, F., Lang, Y., Kermorgant, O., Caro, S.: Cable-driven parallel robot simulation using gazebo and ros. In: ROMANSY 22–Robot Design, Dynamics and Control, pp. 288–295. Springer (2019)
12. Michelin, M., Baradat, C., Nguyen, D.Q., Gouttefarde, M.: Simulation and control with xde and matlab/simulink of a cable-driven parallel robot (cogiro). Mechanisms and Machine Science **32** (08 2015). https://doi.org/10.1007/978-3-319-09489-2_6
13. Coppelia Robotics AG: https://www.coppeliarobotics.com/, online; accessed 21 January 2022
14. Algoryx Simulation: https://www.algoryx.se/, online; accessed 21 January 2022
15. Maplesoft: https://www.maplesoft.com/, online; accessed 21 January 2022
16. Coevoet, E., et al.: Software toolkit for modeling, simulation, and control of soft robots. Advanced Robotics **31**(22), 1208–1224 (2017)
17. Duriez, C., Cotin, S., Lenoir, J., Neumann, P.: New approaches to catheter navigation for interventional radiology simulation. Computer aided surgery **11**(6), 300–308 (2006)
18. Przemieniecki, J.S.: Theory of matrix structural analysis. Courier Corporation (1985)
19. Felippa, C.A., Haugen, B.: A unified formulation of small-strain corotational finite elements: I. theory. Computer Methods in Applied Mechanics and Engineering **194**(21-24), 2285–2335 (2005)
20. Jourdes, F., Valentin, B., Allard, J., Duriez, C., Seeliger, B.: Visual haptic feedback for training of robotic suturing. Frontiers in Robotics and AI **9** (2022)
21. Papailiou, K.O.: On the bending stiffness of transmission line conductors. IEEE Transactions on Power Delivery **12**, 1576–1588 (1997)
22. Mitiguy, P., Banerjee, A.: Determination of spring constants for modeling flexible beams. Working Model Technical Paper (2000), https://www.researchgate.net/publication/265236214
23. Adagolodjo, Y., Renda, F., Duriez, C.: Coupling numerical deformable models in global and reduced coordinates for the simulation of the direct and the inverse kinematics of soft robots. IEEE Robotics and Automation Letters **6**(2), 3910–3917 (2021)
24. Boyer, F., Lebastard, V., Candelier, F., Renda, F.: Dynamics of continuum and soft robots: A strain parameterization based approach. IEEE Transactions on Robotics **37**(3), 847–863 (2020)